JACS
JOURNAL OF THE AMERICAN CHEMICAL SOCIETY
Article
Cite This: J. Am. Chem. Soc. 2019, 141, 3171−3177
pubs.acs.org/JACS

Rational Design of Near-Infrared Aggregation-Induced-Emission-Active Probes: In Situ Mapping of Amyloid-β Plaques with Ultrasensitivity and High-Fidelity

Wei Fu,[†,§] Chenxu Yan,[†,§] Zhiqian Guo,[*,†] Jingjing Zhang,[‡] Haiyan Zhang,[*,‡] He Tian,[†] and Wei-Hong Zhu[*,†]

[†]Key Laboratory for Advanced Materials and Joint International Research Laboratory of Precision Chemistry and Molecular Engineering, Feringa Nobel Prize Scientist Joint Research Center, Shanghai Key Laboratory of Functional Materials Chemistry, Institute of Fine Chemicals, School of Chemistry and Molecular Engineering, East China University of Science and Technology, Shanghai 200237, China

[‡]CAS Key Laboratory of Receptor Research, State Key Laboratory of Drug Research, Shanghai Institute of Materia Medica, Chinese Academy of Sciences, Shanghai 201203, China

Supporting Information

ABSTRACT: High-fidelity mapping of amyloid-β (Aβ) plaques is critical for the early detection of Alzheimer's disease. However, in vivo probing of Aβ plaques by commercially available thioflavin derivatives (ThT or ThS) has proven to be extremely limited, as evident by the restriction of enrichment quenching effect, low signal-to-noise (*S*/*N*) ratio, and poor blood−brain barrier (BBB) penetrability. Herein, we demonstrate a rational design strategy of near-infrared (NIR) aggregation-induced emission (AIE)-active probes for Aβ plaques, through introducing a lipophilic π-conjugated thiophene-bridge for extension to NIR wavelength range with enhancement of BBB penetrability, and tuning the substituted position of the sulfonate group for guaranteeing specific hydrophilicity to maintain the fluorescence-*off* state before binding to Aβ deposition. Probe QM-FN-SO_3 has settled well the AIE dilemma between the lipophilic requirement for longer emission and aggregation behavior from water to protein fibrillogenesis, thus making a breakthrough in high-fidelity feedback on in vivo detection of Aβ plaques with remarkable binding affinity, and serving as an efficient alternative to the commercial probe ThT or ThS.

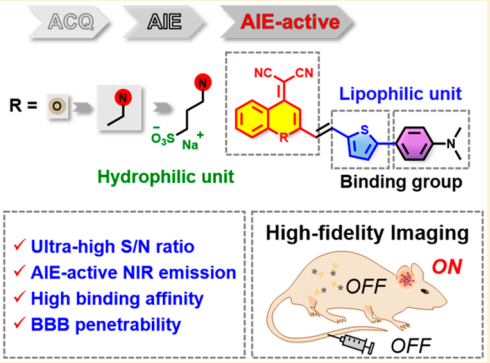

INTRODUCTION

Alzheimer's disease (AD), a progressive neurodegenerative brain disorder, has been considered an incurable condition.[1−5] Like protein fibrillogenesis, the formation and accumulation of amyloid-β (Aβ) plaques in the brain is thought to be a critical pathological hallmark for early diagnosis of AD.[6−12] Commercial thioflavin derivatives (ThT or ThS) are well-known as gold standard probes for in vitro histological staining amyloid fibrils.[13−17] However, the inherent defects including distorted signals from enrichment quenching effect on fluorescence, inevitable noises from *always-on* pattern, and limited blood−brain barrier (BBB) penetrability severely hinder their translation into in vivo imaging (Figure 1A).[18−20] Indeed, it is still far from achieving accurate feedback information for in situ mapping of Aβ plaques.

Aggregation-induced emission (AIE)[21−24] is a preferential strategy to identify protein fibrillogenesis, particularly the light-up characteristic associated with binding events during the aggregation process. The design of such AIE probes, especially extending the wavelength to the NIR region, is essentially required for introducing an additionally hydrophobic π-conjugated bridge.[25−35] However, the undesirable initial aggregation before the probe binding to Aβ aggregates inevitably leads to a "false-positive" AIE signal.[36−39] Therefore, there is an urgent demand to overcome the dilemma between the lipophilic requirement for longer emission and aggregation behavior from water to protein fibrillogenesis. In this regard, we have to increase water solubility of AIE probes to maintain good miscibility in biological media, thus achieving the *off*−*on* fluorescence during the Aβ aggregation process for high sensitivity and fidelity. We envision that NIR AIE-active probes integrating a light-up characteristic in synergy with tunable aggregation behavior could make a breakthrough to directly map Aβ deposition in vivo.

Herein, we describe a molecular rational design strategy to create ultrasensitive *off*−*on* NIR probes for Aβ plaques, relying on the alteration of substituted electron-donating and hydrophilic functional groups to regulate well the aggregated behavior (Figure 1). By virtue of harnessing this strategy, the

Received: November 29, 2018
Published: January 11, 2019

DOI: 10.1021/jacs.8b12820
J. Am. Chem. Soc. 2019, 141, 3171−3177

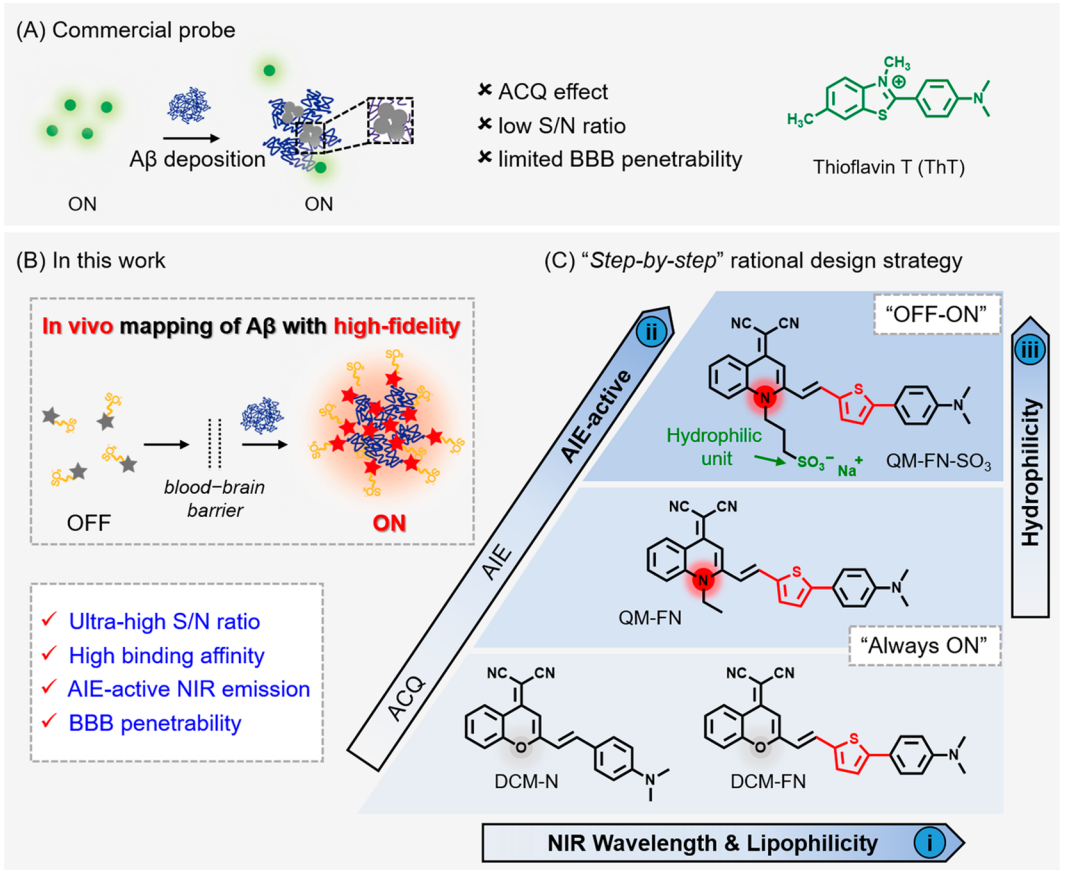

Figure 1. Rational design of NIR AIE-active probes for Aβ deposition. (A) Commercial probe ThT based on the *always-on* pattern. (B, C) The "*step-by-step*" strategy to address the inherent defects of commercial ThT and create ultrasensitive *off*−*on* NIR probes: (i) introducing lipophilic π-conjugated thiophene-bridge for extending the wavelength to the NIR region with BBB penetrability, (ii) replacing the ACQ to AIE building block, and (iii) tuning the sulfonate substituted position for guaranteeing fluorescence-*off* state before binding to Aβ deposition.

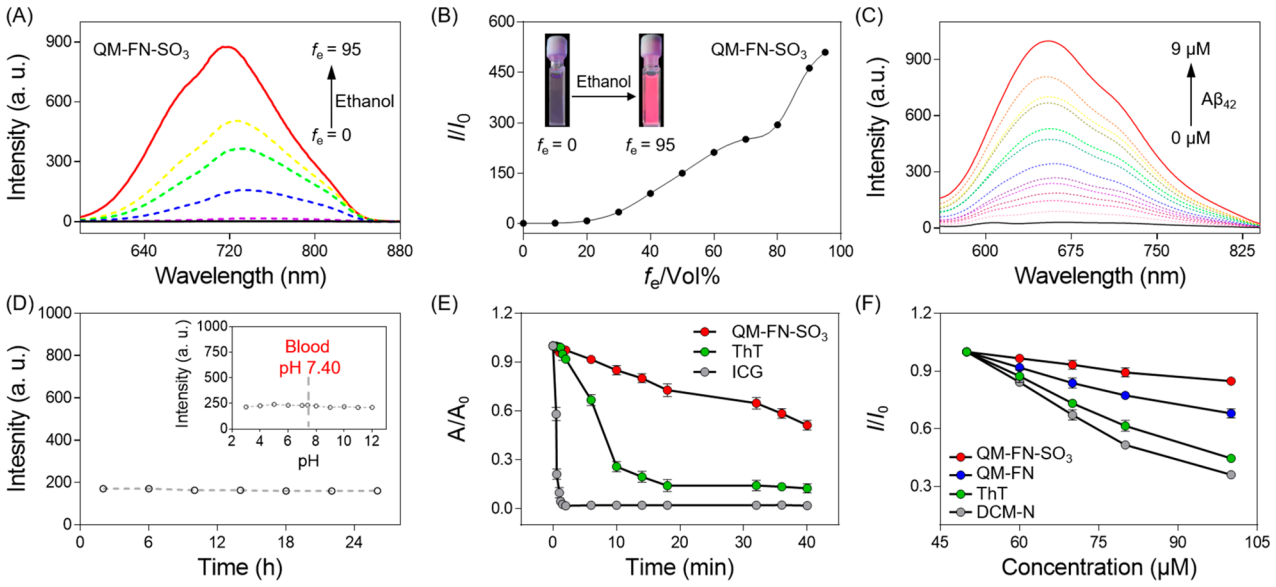

Figure 2. Significant photophysical characteristics of QM-FN-SO_3. (A) Emission spectra of QM-FN-SO_3 in a mixture of water−ethanol with different ethanol fractions (f_e), λ_{ex} = 500 nm. (B) Variations in I/I_0 with f_e, λ_{em} = 720 nm. (C) The fluorescence spectroscopic titration of QM-FN-SO_3 by stepwise addition of Aβ_{42} aggregates (0 to 9 μM) in PBS (pH = 7.4). (D) Fluorescence intensity at 720 nm of QM-FN-SO_3 remaining stable in fresh mouse serum over 24 h at 37 °C and various pH values. (E) Time-dependent absorbance of ICG, ThT, and QM-FN-SO_3 under sustained illumination. (F) Plot of the difference in I/I_0 as a function of the concentration of QM-FN-SO_3, QM-FN, ThT, and DCM-N after response equilibrium with Aβ_{42} aggregates (10 μM).

DOI: 10.1021/jacs.8b12820
J. Am. Chem. Soc. 2019, 141, 3171−3177

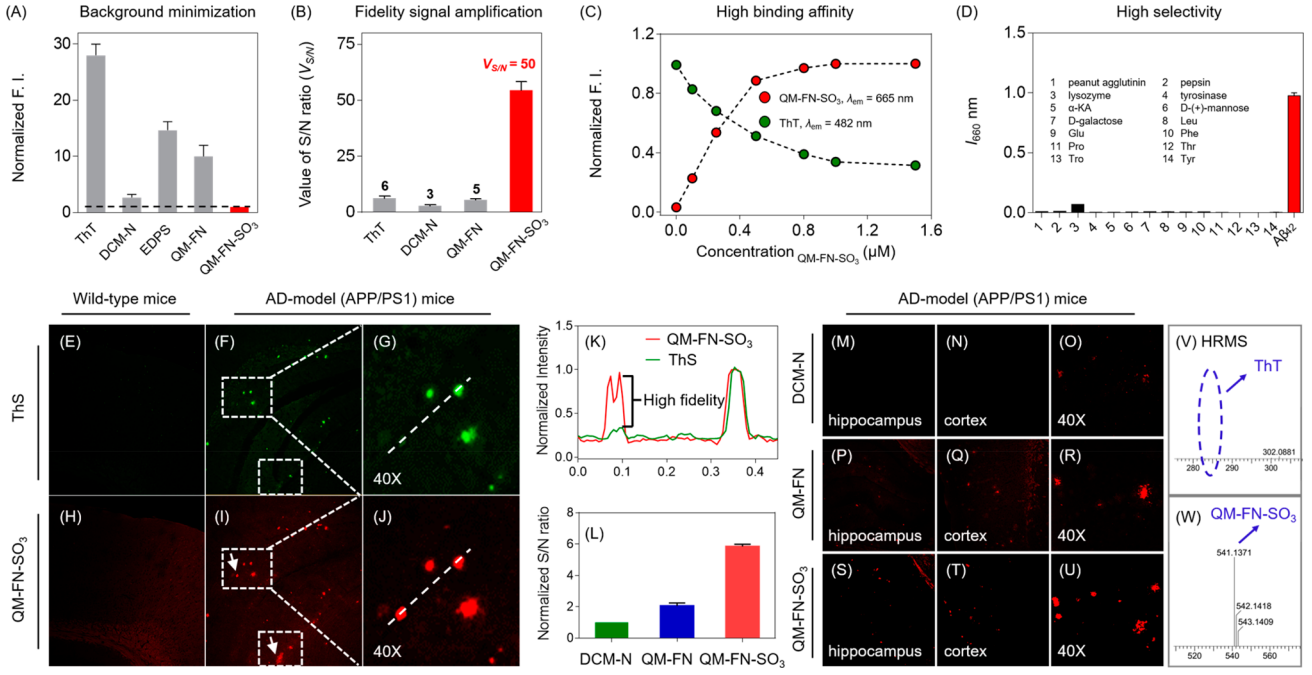

Figure 3. High-fidelity Aβ-driven *off*−*on* NIR responses in solution and brain slices. (A, B) Ultrahigh *S*/*N* ratio of QM-FN-SO_3 combined background minimization, and fidelity signal amplification toward Aβ_{42} aggregates. (C) Remarkable affinity: QM-FN-SO_3 (0−1 μM) effectively displaces ThT from the ThT/Aβ_{42} aggregate complex. (D) High selectivity toward potential competitive species and Aβ_{42} aggregates. (E−J) Histological staining of the brain slices in the hippocampus region from wild-type mice and Alzheimer's disease (AD)-model (APP/PS1 transgenic) mice using ThS and QM-FN-SO_3, respectively. (K) The intensity profiles of the linear regions of interest (ROI) cross the brain slices. (L) The *S*/*N* ratios of DCM-N, QM-FN, and QM-FN-SO_3. (M−U) Adjacent brain sections from APP/PS1 mice stained with DCM-N, QM-FN, and QM-FN-SO_3 in the hippocampus region, the cortex region, and upon magnification of the cortex region (40×), respectively. (V, W) High-resolution mass spectrum extracted from the brain tissue of wild-type mice after 5 min of intravenous injection of probe QM-FN-SO_3 and ThT (2 mg kg^{-1}), respectively.

elaborated probe QM-FN-SO_3 could achieve high-fidelity in situ mapping of Aβ plaques, bestowing the following extraordinary features: (i) ultrahigh signal-to-noise (*S*/*N*) ratio with integrating background minimization and fidelity signal amplification, (ii) remarkable binding affinity to Aβ plaques with efficient BBB penetrability, and (iii) NIR AIE-active emission with excellent photostability. As far as we know, this is the first report of finely tuning molecular aggregation for NIR light-up identifying and binding to Aβ plaques in living mice, even being capable of higher-fidelity mapping than commercial ThT for histological staining.

RESULTS AND DISCUSSION

Rational Design to Regulate Well the Aggregated Behavior. We make full use of the "*step-by-step*" strategy to address the inherent defects of commercial ThT (Figure 1). First, the lipophilic π-conjugated thiophene-bridged unit is covalently attached as extending a π-conjugated backbone for NIR emission and matching the lipophilicity for BBB penetrability. In this case, a significant fluorescent bathochromic shift (~100 nm) was observed from DCM-N to DCM-FN. Sequentially, we focus on our group developed AIE building block (QM, quinoline-malononitrile) to overcome the enrichment quenching effect (from DCM-FN to QM-FN). Finally, and most importantly, we alter the substituted position of the sulfonate group for guaranteeing AIE probes in the fluorescence-*off* state with a minimized background (from QM-FN and EDPS to QM-FN-SO_3, Figure 1 and Scheme S1 in the Supporting Information). Taken together, our strategy could solve well the AIE dilemma between the π-conjugated structure requirement for NIR emission and aggregation behavior, so that the elaborated AIE probe QM-FN-SO_3 performs the desirable *off*−*on* NIR characteristic during the binding to Aβ aggregates.

Significant Enhancement of *S*/*N* Ratio with Integrating Background Minimization and Fidelity Signal Amplification. Unlike the ACQ characteristic of ThT, DCM-N, and DCM-FN (Figures S1−S3 in the Supporting Information), incorporation of the red-emissive QM building block in QM-FN, QM-FN-SO_3, and EDPS (Scheme S1 in the Supporting Information) made them possess unique AIE characteristics.[40,41] However, their aggregated states were significantly different according to the substituent position effect. For example, QM-FN was highly soluble in THF but aggregated in water (Figures S4 and S5 in the Supporting Information). Even though the hydrophilic sulfonate group was introduced into the backbone as a para-substituted electron-donating group, the resulting EDPS (Scheme S1) still exhibited the normal AIE behaviors same as QM-FN.[42] In contrast, upon a change of the sulfonate group into the *N*-substituted position in the QM building block, the exact opposite solvent AIE phenomena were observed from QM-FN-SO_3. Specifically, it was found that water was a good solvent for QM-FN-SO_3, while ethanol was a poor solvent (Figure 2A).

In consequence, QM-FN-SO_3 became nonemissive in aqueous solution, and its NIR fluorescence at 720 nm was continuously intensified until the volume fraction of ethanol (f_e) in the mixed ethanol−water solvent was up to 95% (Figure 2B). Definitely, all these observations demonstrated that the

DOI: 10.1021/jacs.8b12820
J. Am. Chem. Soc. 2019, 141, 3171−3177

distinct aggregation behaviors of these QM-based derivatives were heavily dependent upon the alteration of the sulfonate substituent position with finely regulating hydrophilicity. Here the initial fluorescence-*off* state of QM-FN-SO_3 in aqueous solution and significant enhancement of NIR fluorescence in the aggregated state made it an ideal candidate for mapping protein fibrillogenesis, like Aβ aggregates.

First of all, we investigated whether this AIE-active probe QM-FN-SO_3 could have a fluorescent response upon binding to Aβ aggregates. As shown in Figure 2C, a significant NIR fluorescence enhancement was observed from QM-FN-SO_3 upon association with Aβ_{42} aggregates, and it took ~40 min to reach a plateau (Figure S6 in the Supporting Information). This intensity increase was also accompanied by a blue-shift in the emission spectra. It could be interpreted that QM-FN-SO_3 entered into the hydrophobic pockets and then bound to the aggregated amyloid fibrils with the help of the binding unit *N,N′*-dimethylamino,[43−45] resulting in the decrease of conformational freedom and rotational restriction of QM fluorophore.[46−49] The SEM images of QM-FN-SO_3 without and with Aβ_{42} aggregates further confirmed the binding process (Figure S7 in the Supporting Information). Notably, QM-FN-SO_3 was completely unaffected with pH changes ranging from 3 to 12 and showed excellent stability in fresh serum over 24 h (Figure 2D). Specifically, the time-dependent absorbance of QM-FN-SO_3 upon continuous irradiation demonstrated that it had a much longer half-life time (~2400 s) than those of ThT (~480 s) and ICG (~20 s, FDA-approved NIR contrast agent) (Figure 2E). Obviously, these remarkable characteristics of QM-FN-SO_3 confirmed that it could serve as a high-contrast agent for the detection of Aβ plaques (Figure 2F).

Initial background minimization and fidelity signal amplification of QM-FN-SO_3 were critical for ultrasensitive detection of Aβ plaques. In Figure 3A, in the absence of Aβ, the obviously undesirable background of ThT, DCM-N, and DCM-FN was observed because of their inherent fluorescent properties in aqueous solution. On the other hand, even for AIE-based QM-FN and EDPS, the unexpected AIE-induced background made it difficult for them to really reflect the Aβ plaques, owing to the "false-positive" AIE signal. In fact, QM-FN-SO_3 exhibited a very low background, which was only 1/28, 1/3, 1/15, and 1/10 times those of of ThT, DCM-N, EDPS, and QM-FN, respectively. It could be ascribed to its miscibility in aqueous solution, which thereby minimized the AIE background. Thus, this low background of QM-FN-SO_3 provided a prerequisite for an ultrahigh *S*/*N* ratio. Indeed, QM-FN-SO_3 showed a remarkable *S*/*N* ratio ($V_{S/N}$ = 50) with binding to Aβ_{42} aggregates, far exceeding those of ThT ($V_{S/N}$ = 6), DCM-N ($V_{S/N}$ = 3), and QM-FN ($V_{S/N}$ = 5) (Figure 3B and Figure S8 in the Supporting Information). Definitely, this significant *S*/*N* ratio of QM-FN-SO_3 was acquired by integrating background minimization and fidelity signal amplification.

High Binding Affinity. Importantly, binding affinity was another crucial factor for probes to accurately trace the Aβ plaques. We then elaborated the displacement assay of QM-FN-SO_3 against ThT-bound Aβ_{42} fibrillar aggregates (Figure 3C and Figure S9 in the Supporting Information). Remarkably, with the addition of QM-FN-SO_3 to the ThT/Aβ_{42} aggregated complex, a continuous fluorescence decay of ThT was observed at 482 nm; meanwhile, a corresponding NIR fluorescence enhancement was found at 665 nm, indicating the transformation from ThT/Aβ_{42} to QM-FN-SO_3/Aβ_{42} aggregates. These results demonstrated that QM-FN-SO_3 showed higher binding affinity with Aβ_{42} aggregates than that of ThT. Furthermore, the specificity of QM-FN-SO_3 for Aβ deposition was also evaluated with potentially competitive species including amino acids, enzymes, serum markers, and metabolic substances. As expected, QM-FN-SO_3 did not show any fluorescence response to all these species (Figure 3D), including the Aβ_{42} monomer (Figure S10 in the Supporting Information). Thus, the highly selective NIR fluorescence response of QM-FN-SO_3 with strong binding affinity made it promising for obtaining high-fidelity information, along with initiating the designated *off*−*on* response to Aβ plaques.

With the assistance of the high binding affinity with Aβ plaques (Figure 3C and Figure S11 in the Supporting Information), we further confirmed that QM-FN-SO_3 could completely avoid self-quenching distorted signals from commercially available Aβ probes with a concentration-dependent characteristic.[50−58] As shown in Figure 2F, the binding capacity of the probes with Aβ plaques was investigated. When the probe binding to Aβ deposition was saturated, even further upon addition of probes, the fluorescence intensities of ThT and DCM-N were sharply decreased. In contrast, under the same condition, QM-FN-SO_3 produced only slight changes. It was implied that the AIE effect of QM-FN-SO_3 was highly capable of really reflecting the Aβ plaques with high spatial−temporal feedback, exactly achieving the *off*−*on* behavior with proper water solubility.

In Vitro Mapping with High-Fidelity Aβ Plaque Information. To assess the performance of QM-FN-SO_3 as an alternative to the commercial probes, in vitro fluorescent staining of Aβ plaques in slices of brain tissue from AD-model (APP/PS1 transgenic) mice and wild-type mice was carried out (Figure 3E−U). In fact, commercial Aβ probes such as thioflavin-S (ThS, a gold standard probe for histological staining Aβ plaques) suffered from the limited *S*/*N* ratio due to the inherent initial background and ACQ effect. As anticipated, the specific staining of Aβ plaques was observed in the brain slices of the APP/PS1 mice with probe QM-FN-SO_3 (Figure 3E−J). Notably, the presence and distribution of Aβ plaques were nearly consistent with the results of staining adjacent brain slices using ThS, while there was no obviously plaque labeling in the wild-type mice brain (Figure 3E,H). Impressively, upon quantitatively evaluation of the *S*/*N* ratio of DCM-N, QM-FN, and QM-FN-SO_3 in brain tissues from APP/PS1 transgenic mice (Figure 3M−U), QM-FN-SO_3 showed the highest *S*/*N* ratio over all other probes (Figure 3L). These results demonstrated that QM-FN-SO_3 could specifically in vitro stain Aβ plaques in brain slices.

In particular, QM-FN-SO_3 showed more abundant Aβ plaque feedback than that of ThS. These additional light-up NIR fluorescent signals of QM-FN-SO_3 were discovered (the arrows referred places in Figure 3I,K). In this case, the ACQ effect of ThS could made false signals to some degree, along with inaccurate Aβ deposition feedback, while these were not observed in brain slice staining by ThS (Figure 3F). In contrast, QM-FN-SO_3 could point out and amplify the fidelity signals because of stronger emission during concentration enrichment with Aβ deposition. These in vitro experiment results verified that the *off*−*on* NIR AIE-active probe QM-FN-SO_3 could attain high-fidelity Aβ plaque information in brain tissue slices.

DOI: 10.1021/jacs.8b12820
J. Am. Chem. Soc. 2019, 141, 3171−3177

In Vivo NIR Imaging with BBB Penetrability. Having confirmed Aβ-driven specific NIR light-up responses in brain slices, we further investigated whether this probe could possess desirable biocompatibility for application in living animals. The calculated log *P* values of all probes were acquired to assess the BBB penetrability.[59] Obviously, the log *P* value of QM-FN-SO_3 (1.09) was much higher than that of ThT (0.16), indicative of its potential for matching BBB penetrability. The shaking-flask experiment analysis further confirmed that QM-FN-SO_3 showed better lipophilicity than that of ThT (Figure S12 in the Supporting Information). In fact, via intravenous injection of ThT and QM-FN-SO_3 (perfused with PBS), respectively, high-resolution mass spectrometry from the brain homogenate extraction of wild-type mice could be obtained to verify the BBB penetrability (Figure 3V,W). Clearly, the peak at *m*/*z* 541.1371 (corresponding to $[\text{QM-FN-SO}_3]^-$) was observed while the peak of ThT was not be found from the brain homogenate, demonstrating the BBB penetrability of QM-FN-SO_3.

To further confirm the feasibility of QM-FN-SO_3 for in vivo imaging Aβ plaques, 22-month-old male AD-model (APP/PS1 transgenic) mice and age-matched wild-type mice were employed to observe the brain kinetics by intravenous injection. As shown in Figure 4 and Figure S13 in the Supporting Information, nearly all of the fluorescence signals were centralized in the brain compartments and could be captured very efficiently. In particular, the fluorescence intensity of QM-FN-SO_3 in the brain regions of the APP/PS1 mice was much higher than that in the control of wild-type mice at 20 min after postinjection, indicative of specifically trapping Aβ plaques in vivo with probe QM-FN-SO_3. In addition, the cell viability of the probe QM-FN-SO_3 by the MTT assays demonstrated its favorable biocompatibility (Figure S14 in the Supporting Information). Obviously, these direct visualization results confirmed that QM-FN-SO_3 could cross the blood−brain barrier and label Aβ fibrils in vivo.

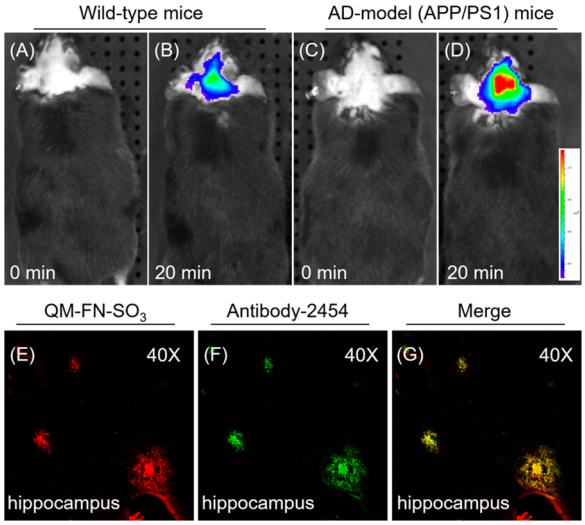

Figure 4. In vivo mapping of Aβ deposition in AD model (APP/PS1 transgenic) mice. Comparison of the fluorescent image at 20 min after intravenous injection of 2.0 mg kg^{-1} of QM-FN-SO_3 into wild-type mice and APP/PS1 mice, n = 3. (E−G) Ex vivo fluorescence observation of brain slices from APP/PS1 mice after injection of probe QM-FN-SO_3. (F) Further confirmation by staining the adjacent sections with antibody-2454. (G) Merged image.

Ex vivo histology of QM-FN-SO_3 binding to Aβ plaques in APP/PS1 transgenic mice was carried out to further validate the in vivo performance. After 20 min of intravenous injection of QM-FN-SO_3, a higher number of Aβ plaques were observed in the brain slices from APP/PS1 mice (Figure 4E). More importantly, we also observed the excellent colocalization of Aβ plaques during staining the same section with anti-Aβ antibody-2454 (Figure 4F). It was further confirmed that the in vivo signal was undoubtedly resulting from QM-FN-SO_3 specifically binding to Aβ plaques.

CONCLUSIONS

In summary, the work focuses on how to develop NIR AIE-active probe QM-FN-SO_3 to circumvent the inherent limitation of commercial probes ThT and ThS, for meeting the high-fidelity requirements to detect Aβ plaques in vivo. In the "*step-by-step*" rational design strategy, we introduced a lipophilic π-conjugated thiophene-bridge, then replaced the ACQ to AIE building block, and finally tuned the substituted position of the sulfonate group. Consequently, probe QM-FN-SO_3 simultaneously eliminated both the self-quenching distorted signal from ThT and the "false-positive" signal from initial aggregation AIE probes before binding to Aβ plaques. In vitro and in vivo experiments provided solid evidence of the accurate feedback of mapping Aβ plaques. We have for the first time solved the dilemma between the lipophilic requirement for NIR emission and aggregation behavior from water to protein fibrillogenesis, making a breakthrough in high-fidelity detection of Aβ plaques. Probe QM-FN-SO_3 exhibited extraordinary features of ultrahigh *S*/*N* ratio, remarkable binding affinity with BBB penetrability, and high-performance NIR emission. This study provides a promising strategy for the design of NIR AIE-active probes, serving as an efficient alternative to the commercial probes, paving a new pathway for insights into protein fibrillogenesis in vivo.

ASSOCIATED CONTENT

Supporting Information

The Supporting Information is available free of charge on the ACS Publications website at DOI: 10.1021/jacs.8b12820.

More detailed experimental procedures, characterizations, and supplementary optical spectra and figures (PDF)

AUTHOR INFORMATION

Corresponding Authors

*whzhu@ecust.edu.cn
*guozq@ecust.edu.cn
*hzhang@simm.ac.cn

ORCID

Zhiqian Guo: 0000-0002-2192-825X
Haiyan Zhang: 0000-0002-2877-2040
He Tian: 0000-0003-3547-7485
Wei-Hong Zhu: 0000-0001-9103-166X

Author Contributions

[§]W.F. and C.Y. contributed equally.

Notes

The authors declare no competing financial interest.

DOI: 10.1021/jacs.8b12820
J. Am. Chem. Soc. 2019, 141, 3171−3177

■ ACKNOWLEDGMENTS

This work was supported by NSFC/China (21788102, 21421004, 21636002, 21622602 and 81522045), National Key Research and Development Program (2017YFC0906902 and 2016YFA0200300), Shanghai Municipal Science and Technology Major Project (Grant 2018SHZDZX03), the Innovation Program of Shanghai Municipal Education Commission, Scientific Committee of Shanghai (15XD1501400), and Programme of Introducing Talents of Discipline to Universities (B16017).

■ REFERENCES

(1) Nesterov, E. E.; Skoch, J.; Hyman, B. T.; Klunk, W. E.; Bacskai, B. J.; Swager, T. M. In vivo optical imaging of amyloid aggregates in brain: design of fluorescent markers. *Angew. Chem., Int. Ed.* **2005**, *44*, 5452.

(2) Gravitz, L. A tangled web of targets. *Nature* **2011**, *475*, S9.

(3) Jakob-Roetne, R.; Jacobsen, H. Alzheimer's disease: from pathology to therapeutic approaches. *Angew. Chem., Int. Ed.* **2009**, *48*, 3030.

(4) Selkoe, D. J. Resolving controversies on the path to Alzheimer's therapeutics. *Nat. Med.* **2011**, *17*, 1060.

(5) Bhasikuttan, A. C.; Mohanty, J. Detection, inhibition and disintegration of amyloid fibrils: the role of optical probes and macrocyclic receptors. *Chem. Commun.* **2017**, *53*, 2789.

(6) Villemagne, V. L.; Dore, V.; Burnham, S. C.; Masters, C. L.; Rowe, C. C. Imaging tau and amyloid-β proteinopathies in Alzheimer disease and other conditions. *Nat. Rev. Neurol.* **2018**, *14*, 225.

(7) Verwilst, P.; Kim, H. S.; Kim, S.; Kang, C.; Kim, J. S. Shedding light on tau protein aggregation: the progress in developing highly selective fluorophores. *Chem. Soc. Rev.* **2018**, *47*, 2249.

(8) Wang, J.; Zhao, C.; Zhao, A.; Li, M.; Ren, J.; Qu, X. New insights in amyloid beta interactions with human telomerase. *J. Am. Chem. Soc.* **2015**, *137*, 1213.

(9) Ni, J. Z.; Taniguchi, A.; Ozawa, S.; Hori, Y.; Kuninobu, Y.; Saito, T.; Saido, T. C.; Tomita, T.; Sohma, Y.; Kanai, M. Near-infrared photoactivatable oxygenation catalysts of amyloid peptide. *Chem.* **2018**, *4*, 807.

(10) Hardy, J.; Selkoe, D. J. The amyloid hypothesis of Alzheimer's disease: progress and problems on the road to therapeutics. *Science* **2002**, *297*, 353.

(11) Cao, K. J.; Yang, J. Translational opportunities for amyloid-targeting fluorophores. *Chem. Commun.* **2018**, *54*, 9107.

(12) Kung, H. F. The β-amyloid hypothesis in Alzheimer's disease: seeing is believing. *ACS Med. Chem. Lett.* **2012**, *3*, 265.

(13) Hong, Y.; Meng, L.; Chen, S.; Leung, C. W.; Da, L. T.; Faisal, M.; Silva, D. A.; Liu, J.; Lam, J. W.; Huang, X.; Tang, B. Z. Monitoring and inhibition of insulin fibrillation by a small organic fluorogen with aggregation-induced emission characteristics. *J. Am. Chem. Soc.* **2012**, *134*, 1680.

(14) Amdursky, N.; Erez, Y.; Huppert, D. Molecular rotors: what lies behind the high sensitivity of the Thioflavin-T fluorescent marker. *Acc. Chem. Res.* **2012**, *45*, 1548.

(15) Groenning, M. Binding mode of Thioflavin T and other molecular probes in the context of amyloid fibrils-current status. *J. Chem. Biol.* **2010**, *3*, 1.

(16) Biancalana, M.; Koide, S. Molecular mechanism of Thioflavin-T binding to amyloid fibrils. *Biochim. Biophys. Acta, Proteins Proteomics* **2010**, *1804*, 1405.

(17) Rodriguez-Rodriguez, C.; Rimola, A.; Rodriguez-Santiago, L.; Ugliengo, P.; Alvarez-Larena, A.; Gutierrez-de-Teran, H.; Sodupe, M.; Gonzalez-Duarte, P. Crystal structure of thioflavin-T and its binding to amyloid fibrils: insights at the molecular level. *Chem. Commun.* **2010**, *46*, 1156.

(18) Mora, A. K.; Singh, P. K.; Patro, B. S.; Nath, S. PicoGreen: a better amyloid probe than Thioflavin-T. *Chem. Commun.* **2016**, *52*, 12163.

(19) Kuznetsova, I. M.; Sulatskaya, A. I.; Uversky, V. N.; Turoverov, K. K. Analyzing Thioflavin T binding to amyloid fibrils by an equilibrium Microdialysis-based technique. *PLoS One* **2012**, *7*, No. e30724.

(20) Dzwolak, W.; Pecul, M. Chiral bias of amyloid fibrils revealed by the twisted conformation of Thioflavin T: An induced circular dichroism/DFT study. *FEBS Lett.* **2005**, *579*, 6601.

(21) Wang, Y.-L.; Fan, C.; Xin, B.; Zhang, J.-P.; Luo, T.; Chen, Z.-Q.; Zhou, Q.-Y.; Yu, Q.; Li, X.-N.; Huang, Z.-L.; Li, C.; Zhu, M.-Q.; Tang, B. Z. AIE-based super-resolution imaging probes for β-amyloid plaques in mouse brains. *Mater. Chem. Front.* **2018**, *2*, 1554.

(22) Mei, J.; Leung, N. L.; Kwok, R. T.; Lam, J. W.; Tang, B. Z. Aggregation-induced emission: together we shine, united we soar. *Chem. Rev.* **2015**, *115*, 11718.

(23) Feng, G.; Liu, B. Aggregation-induced emission (AIE) dots: emerging theranostic nanolights. *Acc. Chem. Res.* **2018**, *51*, 1404.

(24) Xie, S.; Wong, A. Y. H.; Kwok, R. T. K.; Li, Y.; Su, H.; Lam, J. W. Y.; Chen, S.; Tang, B. Z. Fluorogenic Ag^{+}-tetrazolate aggregation enables novel and efficient fluorescent biological silver staining. *Angew. Chem., Int. Ed.* **2018**, *57*, 5750.

(25) Chevalier, A.; Zhang, Y.; Khdour, O. M.; Kaye, J. B.; Hecht, S. M. Mitochondrial nitroreductase activity enables selective imaging and therapeutic targeting. *J. Am. Chem. Soc.* **2016**, *138*, 12009.

(26) Li, X.; Kwon, N.; Guo, T.; Liu, Z.; Yoon, J. Innovative strategies for hypoxic-tumor photodynamic therapy. *Angew. Chem., Int. Ed.* **2018**, *57*, 11522.

(27) Yan, C.; Guo, Z.; Liu, Y.; Shi, P.; Tian, H.; Zhu, W. H. A sequence-activated AND logic dual-channel fluorescent probe for tracking programmable drug release. *Chem. Sci.* **2018**, *9*, 6176.

(28) Guo, Z.; Park, S.; Yoon, J.; Shin, I. Recent progress in the development of near-infrared fluorescent probes for bioimaging applications. *Chem. Soc. Rev.* **2014**, *43*, 16.

(29) Yan, J.; Lee, S.; Zhang, A.; Yoon, J. Self-immolative colorimetric, fluorescent and chemiluminescent chemosensors. *Chem. Soc. Rev.* **2018**, *47*, 6900.

(30) Lee, M. H.; Kim, J. S.; Sessler, J. L. Small molecule-based ratiometric fluorescence probes for cations, anions, and biomolecules. *Chem. Soc. Rev.* **2015**, *44*, 4185.

(31) Andreasson, J.; Pischel, U. Molecules for security measures: from keypad locks to advanced communication protocols. *Chem. Soc. Rev.* **2018**, *47*, 2266.

(32) Wu, D.; Sedgwick, A. C.; Gunnlaugsson, T.; Akkaya, E. U.; Yoon, J.; James, T. D. Fluorescent chemosensors: the past, present and future. *Chem. Soc. Rev.* **2017**, *46*, 7105.

(33) Li, L.; Zhang, C. W.; Chen, G. Y.; Zhu, B.; Chai, C.; Xu, Q. H.; Tan, E. K.; Zhu, Q.; Lim, K. L.; Yao, S. Q. A sensitive two-photon probe to selectively detect monoamine oxidase B activity in Parkinson's disease models. *Nat. Commun.* **2014**, *5*, 3276.

(34) Watanabe, H.; Ono, M.; Saji, H. In vivo fluorescence imaging of β-amyloid plaques with push-pull dimethylaminothiophene derivatives. *Chem. Commun.* **2015**, *51*, 17124.

(35) Qian, L. H.; Fu, J. Q.; Yuan, P. Y.; Du, S. B.; Huang, W.; Li, L.; Yao, S. Q. Intracellular delivery of native proteins facilitated by cell-penetrating poly(disulfide)s. *Angew. Chem., Int. Ed.* **2018**, *57*, 1532.

(36) Gunnlaugsson, T. Accessible self-assembly. *Nat. Chem.* **2016**, *8*, 6.

(37) Yu, C. Y.; Xu, H.; Ji, S.; Kwok, R. T.; Lam, J. W.; Li, X.; Krishnan, S.; Ding, D.; Tang, B. Z. Mitochondrion-anchoring photosensitizer with aggregation-induced emission characteristics synergistically boosts the radiosensitivity of cancer cells to ionizing radiation. *Adv. Mater.* **2017**, *29*, 1606167.

(38) Yuan, Y.; Kwok, R. T.; Tang, B. Z.; Liu, B. Targeted theranostic platinum(IV) prodrug with a built-in aggregation-induced emission light-up apoptosis sensor for noninvasive early evaluation of its therapeutic responses in situ. *J. Am. Chem. Soc.* **2014**, *136*, 2546.

(39) Liu, H. W.; Li, K.; Hu, X. X.; Zhu, L.; Rong, Q.; Liu, Y.; Zhang, X. B.; Hasserodt, J.; Qu, F. L.; Tan, W. In situ localization of enzyme activity in live cells by a molecular probe releasing a precipitating fluorochrome. *Angew. Chem., Int. Ed.* **2017**, *56*, 11788.

DOI: 10.1021/jacs.8b12820
J. Am. Chem. Soc. 2019, 141, 3171−3177

(40) Shao, A.; Xie, Y.; Zhu, S.; Guo, Z.; Zhu, S.; Guo, J.; Shi, P.; James, T. D.; Tian, H.; Zhu, W. H. Far-red and near-IR AIE-active fluorescent organic nanoprobes with enhanced tumor-targeting efficacy: shape-specific effects. *Angew. Chem., Int. Ed.* **2015**, *54*, 7275.
(41) Gu, K.; Qiu, W.; Guo, Z.; Yan, C.; Zhu, S.; Yao, D.; Shi, P.; Tian, H.; Zhu, W.-H. An enzyme-activatable probe liberating AIEgens: on-site sensing and long-term tracking of β-galactosidase in ovarian cancer cells. *Chem. Sci.* **2019**, *10*, 398.
(42) Shao, A. D.; Guo, Z. Q.; Zhu, S. J.; Zhu, S. Q.; Shi, P.; Tian, H.; Zhu, W. H. Insight into aggregation-induced emission characteristics of red-emissive quinolinemalononitrile by cell tracking and real-time trypsin detection. *Chem. Sci.* **2014**, *5*, 1383.
(43) Verwilst, P.; Kim, H. R.; Seo, J.; Sohn, N. W.; Cha, S. Y.; Kim, Y.; Maeng, S.; Shin, J. W.; Kwak, J. H.; Kang, C.; Kim, J. S. Rational design of in vivo tau tangle-selective near-infrared fluorophores: expanding the BODIPY universe. *J. Am. Chem. Soc.* **2017**, *139*, 13393.
(44) Cai, L.; Innis, R.; Pike, V. Radioligand development for PET imaging of β-amyloid (Aβ)-current status. *Curr. Med. Chem.* **2007**, *14*, 19.
(45) Kim, D.; Baik, S. H.; Kang, S.; Cho, S. W.; Bae, J.; Cha, M. Y.; Sailor, M. J.; Mook-Jung, I.; Ahn, K. H. Close correlation of monoamine oxidase activity with progress of Alzheimer's disease in mice, observed by in vivo two-photon imaging. *ACS Cent. Sci.* **2016**, *2*, 967.
(46) Sedgwick, A.; Dou, W. T.; Jiao, J. B.; Wu, L.; Williams, G. T.; Jenkins, A. T. A.; Bull, S. D.; Sessler, J. L.; He, X. P.; James, T. D. An ESIPT probe for the ratiometric imaging of peroxynitrite facilitated by binding to Aβ-aggregates. *J. Am. Chem. Soc.* **2018**, *140*, 14267−14271.
(47) Zhang, X.; Tian, Y.; Li, Z.; Tian, X.; Sun, H.; Liu, H.; Moore, A.; Ran, C. Design and synthesis of curcumin analogues for in vivo fluorescence imaging and inhibiting copper-induced cross-linking of amyloid beta species in Alzheimer's disease. *J. Am. Chem. Soc.* **2013**, *135*, 16397.
(48) Hintersteiner, M.; Enz, A.; Frey, P.; Jaton, A. L.; Kinzy, W.; Kneuer, R.; Neumann, U.; Rudin, M.; Staufenbiel, M.; Stoeckli, M.; Wiederhold, K. H.; Gremlich, H. U. In vivo detection of amyloid-β deposits by near-infrared imaging using an oxazine-derivative probe. *Nat. Biotechnol.* **2005**, *23*, 577.
(49) Cui, M.; Ono, M.; Watanabe, H.; Kimura, H.; Liu, B.; Saji, H. Smart near-infrared fluorescence probes with donor-acceptor structure for in vivo detection of β-amyloid deposits. *J. Am. Chem. Soc.* **2014**, *136*, 3388.
(50) Teng, I. T.; Li, X.; Yadikar, H. A.; Yang, Z.; Li, L.; Lyu, Y.; Pan, X.; Wang, K. K.; Tan, W. Identification and characterization of DNA aptamers specific for phosphorylation epitopes of tau protein. *J. Am. Chem. Soc.* **2018**, *140*, 14314.
(51) Lv, G.; Sun, A.; Wei, P.; Zhang, N.; Lan, H.; Yi, T. A spiropyran-based fluorescent probe for the specific detection of β-amyloid peptide oligomers in Alzheimer's disease. *Chem. Commun.* **2016**, *52*, 8865.
(52) Cheng, Y.; Zhu, B.; Deng, Y.; Zhang, Z. In vivo detection of cerebral amyloid fibrils with smart dicynomethylene-4H-pyran-based fluorescence probe. *Anal. Chem.* **2015**, *87*, 4781.
(53) Zhou, K.; Bai, H.; Feng, L.; Dai, J.; Cui, M. Smart D-π-A type near-infrared Aβ probes: effects of a marked π bridge on optical and biological properties. *Anal. Chem.* **2017**, *89*, 9432.
(54) Li, Y.; Yang, J.; Liu, H.; Yang, J.; Du, L.; Feng, H.; Tian, Y.; Cao, J.; Ran, C. Tuning the stereo-hindrance of a curcumin scaffold for the selective imaging of the soluble forms of amyloid beta species. *Chem. Sci.* **2017**, *8*, 7710.
(55) Kim, D.; Moon, H.; Baik, S. H.; Singha, S.; Jun, Y. W.; Wang, T.; Kim, K. H.; Park, B. S.; Jung, J.; Mook-Jung, I.; Ahn, K. H. Two-photon absorbing dyes with minimal autofluorescence in tissue imaging: application to in vivo imaging of amyloid-β plaques with a negligible background signal. *J. Am. Chem. Soc.* **2015**, *137*, 6781.
(56) Teoh, C. L.; Su, D.; Sahu, S.; Yun, S. W.; Drummond, E.; Prelli, F.; Lim, S.; Cho, S.; Ham, S.; Wisniewski, T.; Chang, Y. T. Chemical fluorescent probe for detection of Aβ oligomers. *J. Am. Chem. Soc.* **2015**, *137*, 13503.
(57) Staderini, M.; Martin, M. A.; Bolognesi, M. L.; Menendez, J. C. Imaging of β-amyloid plaques by near infrared fluorescent tracers: a new frontier for chemical neuroscience. *Chem. Soc. Rev.* **2015**, *44*, 1807.
(58) Cao, K.; Farahi, M.; Dakanali, M.; Chang, W. M.; Sigurdson, C. J.; Theodorakis, E. A.; Yang, J. Aminonaphthalene 2-cyanoacrylate (ANCA) probes fluorescently discriminate between amyloid-β and prion plaques in brain. *J. Am. Chem. Soc.* **2012**, *134*, 17338.
(59) Ametamey, S. M.; Honer, M.; Schubiger, P. A. Molecular imaging with PET. *Chem. Rev.* **2008**, *108*, 1501.

DOI: 10.1021/jacs.8b12820
J. Am. Chem. Soc. 2019, 141, 3171−3177